Effect of chemical and physical factors on the crystallization of calcium sulfate in seawater reverse osmosis brine

Youngkwon Choi[a], Gayathri Naidu[a], Sanghyun Jeong[b, *], Sangho Lee[c], Saravanamuthu Vigneswaran[a,*]

[a]Faculty of Engineering, University of Technology Sydney (UTS), P.O Box 123, Broadway, NSW 2007 Australia,

[b]Graduate School of Water Resources, Sungkyunkwan University (SKKU), 2066, Seobu-ro, Jangan-gu, Suwon-si, Gyeonggi-do, 16419, Republic of Korea

[c]School of Civil and Environmental Engineering, Kookmin University, Seoul 136-702, Republic of Korea

*Corresponding authors: S. Jeong (Tel +82-31-290-5498; Fax: +82-31-290-7549; Email: sh.jeong@skku.edu), S. Vigneswaran (Tel +61-2-9514-2641; Fax +61-2-9514-2633; Email: Saravanamuth.Vigneswaran@uts.edu.au)

Abstract

A major challenge of the seawater reverse osmosis (SWRO) desalination process corresponds to the management of concentrated brine waste because discharging the brine back into the sea through submarine pipelines influences the marine ecosystem and incurs additional costs at coastal RO plants. A membrane distillation crystallizer (MDC) can further produce clean water and simultaneously recover valuable resources from the concentrated brine; this is more environmentally and economically optimal. The SWRO brine contains salts, which contribute to scaling development during the MDC operation. Hence, the main goals of this study include (i) observing the crystallization tendency of calcium sulfate ($CaSO_4$) under high salinity and, (ii) examining other inorganic and organic compounds and operational conditions that affect the $CaSO_4$ crystallization. The crystallization tendency of $CaSO_4$ in SWRO brine

23 was examined with respect to different temperatures; changes in pH values; and in the presence

24 of co-existing ions, chemical agents, and organic matters as well as physical factors. The results

25 showed that the size and quantity of crystals formed increased with increasing heating

26 temperatures. Furthermore, an increase in the pH values (from 5 to 9) increased the crystal size.

27 At higher pH, the complexion of NaCl along with $CaSO_4$ was created. Moreover, stirring

28 enhanced $CaSO_4$ crystal formation due to the kinetic mechanism.

29 **Keywords**: Calcium sulfate; Crystallization; Membrane distillation crystallizer; Seawater

30 reverse osmosis brine

31

1.   Introduction

33   The demand for desalination technology based on seawater reverse osmosis (SWRO)

34 process is continuously increasing with the global lack of potable water [1, 2]. However,

35 SWRO generates a high amount of concentrated brine containing high salt concentration that

36 causes serious environmental issues [3]. The treatment or disposal methods of SWRO brine are

37 highly dependent on the location of the SWRO plant. For example, an inland SWRO plant

38 requires brine disposal methods such as an evaporation pond and deep well injection. When

39 SWRO brine is directly discharged into seawater, additional facilities are required to transport

40 it, thereby incurring additional operational costs. Furthermore, the direct discharge of SWRO

41 brine to sea influences the marine eco-system due to the high concentration of salt and

42 chemicals in the SWRO brine [4]. Extant studies reported on the contamination of soil, ground

43 water, and the marine eco-system by brine [4, 5]. Several researchers tested alternative methods

44 for brine treatment and used methods mainly based on membrane technologies, such as forward

45 osmosis (FO), pressure retarded osmosis (PRO), and membrane distillation (MD), to recover

46 valuable resources or energy from the brine while producing water, and subsequently resulting

47 in the reduction of environmentally negative effect of brine on the ecosystem [6-13].

48　　　　The MD process is a promising technology for treating high salinity solution such as

49 SWRO brine [12-14]. This is because MD is a mechanically and thermally driven desalination

50 process that is operated by the vapor pressure difference between hot feed solution and cool

51 permeate solution flowing across a micro-porous hydrophobic membrane. Thus, the effect of

52 solution concentration on permeate flux is less than that of the other desalination processes [3,

53 15]. Additionally, MD possesses several advantages including high rejection of non-volatile

54 components, lower operational pressure when compared to that of reverse osmosis (RO), and

55 lower operating temperature and smaller footprints when compared to those of conventional

56 distillation processes [16-18]. Recently, a novel combined process, namely MD with a

57 crystallizer (MDC), is highlighted with an increase in the interest to recover valuable resources

58 from seawater [3, 19-23].

59　　　　Specifically, SWRO brine contains a higher concentration of valuable resources when

60 compared to feed water (seawater). During the crystallization process, salts in the SWRO brine

61 can be separated and used as a valuable resource. However, although these salts may be used

62 as valuable resources, they may display a negative influence at high concentrations and

63 especially when they are treated by using conventional treatment methods [24]. The application

64 of MD enables in achieving a highly concentrated brine, and thereby generating a super-

65 saturation state for crystallization [25]. Theoretically, MD concentrates the feed solution to

66 create a super-saturated solution to form crystals [22]. Meanwhile, the crystallization part of

67 MDC mitigates the scaling phenomenon on membrane surface because salts are continuously

68 removed as solid crystals in the crystallizer [19, 26].

69　　　　Despite the high potential of the MDC, fouling and scaling phenomena are inevitable.

70　　These phenomena are more evident with the SWRO brine treatment when compared to the

71　　desalination process [19, 27]. The SWRO brine contains calcium (Ca^{2+}) based crystalline

72　　matters with a high concentration; calcium sulfate ($CaSO_4$) and calcium carbonate ($CaCO_3$)

73　　that possess low solubility [28]. Thus, Ca^{2+} based crystalline matters first precipitate in the

74　　form of crystals prior to reaching a super-saturation state of the target material. Hence, the

75　　surface and pores of the MD membrane can be covered by these sparingly soluble salts [29].

76　　Previous studies investigated the scaling of $CaSO_4$ and $CaCO_3$ in the MD process [13, 30]. He

77　　et al. (2009) examined the effect of temperature and feed flow velocity on crystallization

78　　tendency in a direct contact membrane distillation (DCMD) process. Curcio et al. (2009)

79　　investigated the interaction between $CaCO_3$ crystallization and biofouling in a high salinity

80　　solution. However, there is a lack of fundamental studies on the salts crystallization tendency

81　　due to various factors because most studies on Ca^{2+} scaling and fouling phenomenon focus on

82　　the membrane surface. It is important to understand Ca^{2+} crystallization tendency in terms of

83　　the influence of chemicals and physical factors.

84　　　　　The characteristics of SWRO brine depend on feed water quality, the recovery ratio of

85　　the SWRO process, the pre-treatment methods of feed water, and the chemical cleaning

86　　methods of the membrane [1, 31-33]. The SWRO brine contains various ions and chemical

87　　components that are used in the pre-treatment processes and during membrane chemical

88　　washing in the RO process. Additionally, the concentration of these ions in the brine is double

89　　or higher than that in feed water [33]. The ionic interaction among the ions leads to the

90　　crystallization propensity of $CaSO_4$ in the SWRO brine. Therefore, it is important to understand

91　　the influence of all ions on the crystallization tendency of $CaSO_4$ for the stable operation of the

92　　MDC process. This also obtains reliable information on the ionic interaction for $CaSO_4$

93   crystallization because it can act as a major foulant in the MD part of MDC process, thereby

94   resulting in the degradation of process performance [34]. Moreover, physical factors, such as

95   agitation (in feed tank) and stirring speed, can affect crystallization during the MDC process

96   [35].

97   Thus, the present study investigates the crystallization tendency of $CaSO_4$ in the SWRO

98   brine for different conditions: temperatures (50-80 ℃) and pH values (5-9). The study also

99   examined the effect of (1) chemical factors (temperature, pH, NaCl concentration, and

100   chemical agents); (2) organic matters (alginate (AA), humic acid (HA), and bovine serum

101   albumin (BSA)); and (3) physical factors (agitation) on the $CaSO_4$ crystallization. The crystal

102   growth was evaluated in terms of the crystal size distribution (CSD) and calcium ion (Ca^{2+})

103   removal efficiency (variation in the Ca^{2+} concentration before and after the crystallization).

2. Materials and Methods

2.1 Preparation of feed solution

In order to observe $CaSO_4$ crystallization phenomenon in the high salinity solution, a synthetic feed solution containing high concentrations of calcium (Ca^{2+}) and sulfate (SO_4^{2-}) ions as approximately twice as seawater (to represent 50% recovered real SWRO brine) was prepared [36]. The stock solutions of sodium chloride (NaCl), sodium sulfate (Na_2SO_4), and calcium chloride dihydrate ($CaCl_2 \cdot 2H_2O$) were prepared and used as a feed solution, and its composition is specified in **Table 1**.

Table 1 Composition of the synthetic feed solution for the $CaSO_4$ crystallization experiment.

Ions	Concentration (mg/L)
Calcium (Ca^{2+})	1,620
Sodium (Na^+)	51,460
Chloride (Cl^-)	73,770
Sulfate (SO_4^{2-})	11,520

2.2 Batch crystallization experiment

In order to examine the tendency of $CaSO_4$ crystallization in the concentrated brine, batch experiments were conducted under same standard conditions with the exception of a single parameter that was changed to examine the effect of the specific parameter on crystal formation. The feed corresponds to a mixed solution of NaCl, Na_2SO_4, and $CaCl_2 \cdot 2H_2O$. Given all the ions that are present, Ca^{2+} and SO_4^{2-} are combined by an ionic electric bond force and precipitation in the form of $CaSO_4$ crystals (**Figure 1**). The crystallization phenomenon is

6

influenced by chemical and physical factors. Hence, all experimental sets were initially

122 conducted at a standard condition (heating temperature: 60 °C, pH 7, and stirring speeds: 200

123 and 50 rpm). The high speed (200 rpm) was to homogeneous the solution and lower speed of

124 50 rpm was to generate a crystallization. The temperature, pH value, and stirring speed

125 conditions were altered to examine the effect of them individually on crystallization. In order

126 to examine the effect of temperature on $CaSO_4$ crystallization, feed solutions were heated in a

127 water bath set at the following temperatures: 50 °C, 60 °C, and 80 °C.

128   Essentially, a heating temperature of 60 °C was used and first tested with synthetic feed

129 solution as shown in **Table 1**. A 500 mL feed solution was prepared in a beaker with pH

130 adjusted by using 0.1M HCl and 0.1M NaOH. In order to examine the effect of temperature on

131 $CaSO_4$ crystallization, feed solutions were heated in a water bath set at the following

132 temperatures: 50 °C, 60 °C, and 80 °C. Subsequently, feed solutions were mixed in a jar-tester

133 at a high speed (200 rpm) for 2 min for complete mixing and then allowed to stand for 24 h at

134 a room temperature with a stirring at low speed (50 rpm) for continuous mixing while

135 facilitating crystallization. After 24 h, the crystals were separated from the solution by using a

136 glass microfiber filter (Whatman, Grade GF/C, pore: 1.2 μm).

Crystallization procedure   Analysis
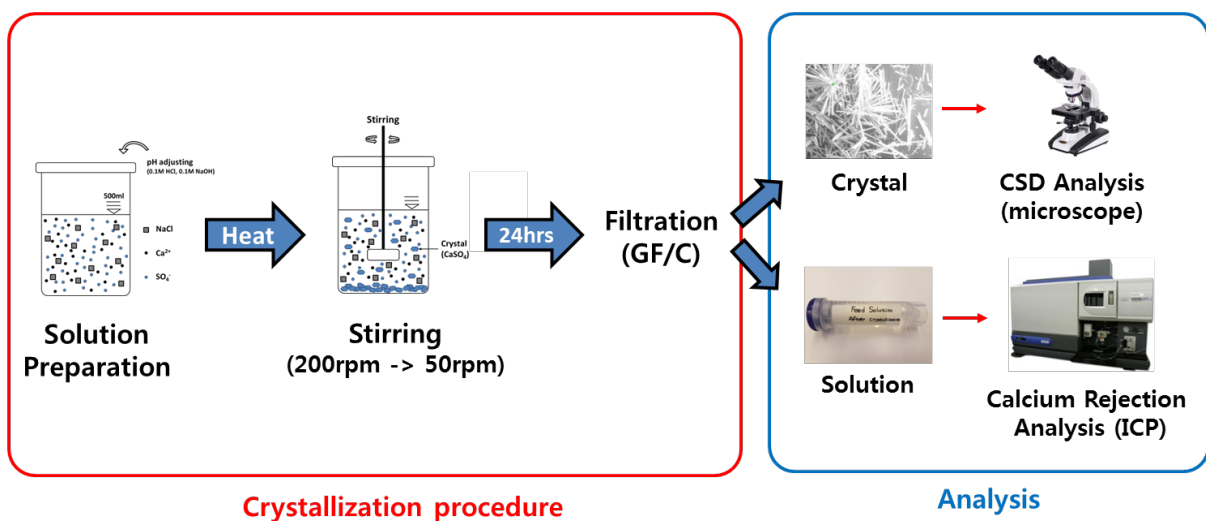
137

138 **Figure 1**   Crystallization procedure and analysis.

139

140 **2.3 Chemicals and solutions**

141 **2.3.1   CaSO₄ with other ions**

142   The effect of other ions on $CaSO_4$ crystallization was investigated with sodium chloride

143 (NaCl), bicarbonate (HCO_3^-) (by using sodium bicarbonate ($NaHCO_3$)), magnesium (Mg^{2+})

144 (by using magnesium chloride hexahydrate ($MgCl_2 \cdot 6H_2O$)), and potassium (K^+) (by using

145 potassium chloride (KCl)).

146 **2.3.2   Chemical washing agent**

147   The effect of alkaline reagents of ethylene diamine tetraacetic acid (EDTA) was used

148 as a chemical washing agent in the membrane of a SWRO desalination plant to remove fouling

149 on the membrane surface [37, 38].

150 **2.3.3   Coagulant**

151   Coagulation decreases biological materials in the feed water of the water treatment

152 process and results in the reduction of biofouling potential to remove polysaccharide-like and

153 protein-like organic matters [39]. The coagulants used in the study included $FeSO_4$ and $FeCl_3$,

154 which were known as effective primary coagulants to neutralize the electric charges of particles

155 in the water and cause the particles to attach together [40]. Typically, the coagulation chemicals

156 that are used correspond to ferrous sulfate ($FeSO_4$) and ferric chloride ($FeCl_3$)). The effect of

157 the above chemicals on $CaSO_4$ crystallization was also examined.

8

2.3.4 Organic matter

The effect of organic matter on CaSO$_4$ crystallization in high salinity was also examined with model organic compounds of alginate (AA) (A7003, CAS NO. 9005-32-7, Sigma-Aldrich, St. Louis, MO), humic acid (HA) (53680, CAS No. 1415-93-6, Sigma-Aldrich, St. Louis, MO), and bovine serum albumin (BSA) (A2135, CAS No. 9048-46-8, Sigma-Aldrich, St. Louis, MO) to represent polysaccharides, humics, and proteins, respectively.

2.4 Physical factors

In both the water treatment process and the crystallization process, the mixing methods (physical mixer and aeration) are performed to maintain a homogeneous solution without polarization in a reactor and mitigate the membrane fouling of a membrane on the water treatment process. The application of physical devices generates kinetic energy and affects the formation and growth of CaSO$_4$ crystals in the solution [35]. In the study, agitation (stirring) was used to evaluate the effect of mixing (intensity) on the CaSO$_4$ crystallization tendency. Agitation was applied in a jar tester at different speeds (0 rpm, 20 rpm, and 150 rpm) following a high speed (200 rpm for 2 min). Different stirring speeds (0 rpm, 20 rpm, and 150 rpm) were set to investigate the effect of mixing speed on the CaSO$_4$ crystallization.

2.5 Analyses

Crystals generated with different factors at same standard condition were analyzed by using a field emission scanning electron microscopy-energy dispersive X-ray (FESEM-EDX,

179   Zeiss supra 55VP, Carl Zeiss AG) to examine the variation of crystal morphology and to

180   identify the type of crystals. Inductively coupled plasma optical emission spectrometry (ICP-

181   OES, Optima7300DV- ICP-OES Perkin Elmer, US) was used to examine the variation in the

182   ionic concentration in the feed following crystallization to measure the degree of forming

183    $CaSO_4$ crystals. Furthermore, a microscopy method was used to measure crystal size

184   distribution (CSD). At least 150 crystals were randomly selected, and crystals were sized by

185   microscopy with an image analyzer (ImagePro7).

3. Results and Discussion

3.1 CaSO₄ crystal formation

Generally, the CaSO$_4$ crystal has six sides that enable it to grow in six directions as shown in **Figure 2** [41]. In the study, for the purposes of simplicity, only growths in two directions were considered, namely [001] and [100]. Directions [001] and [100] are referred to as 'Length' and 'Width', respectively.

Visible salt/crystal formation occurred during the experiment. The SEM-EDX analysis established the formation of CaSO$_4$ crystals (**Figure 3 (a)**). Based on the crystal size distribution (CSD) analysis (**Figure 3 (b) and (c)**), the CaSO$_4$ crystal length was in the range of 50-1000 μm with a width in the range of 10-140 μm. The CSD results indicated that the growth rate and comparative size of the CaSO$_4$ crystals differed in the "Length" and "Width" directions. The growth rate towards the "Length" direction and comparative maximum size was faster and larger than those in the "Width" direction. Based on the initial and final Ca^{2+} concentrations of the solution (initial: 1,620 mg/L, and final: 1,158 mg/L), 28.5% Ca^{2+} removal efficiency was detected. The reduction/removal of Ca^{2+} was attributed to the CaSO$_4$ formation and precipitation.

11
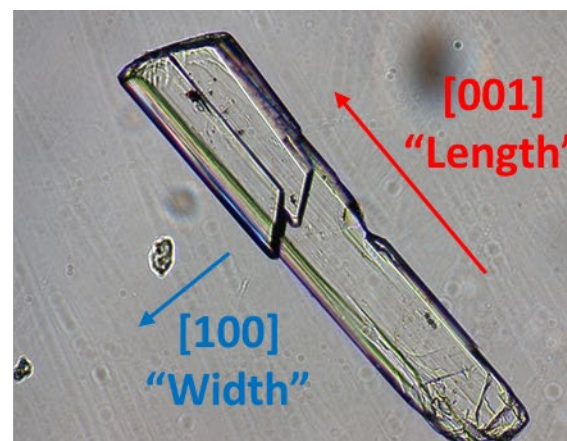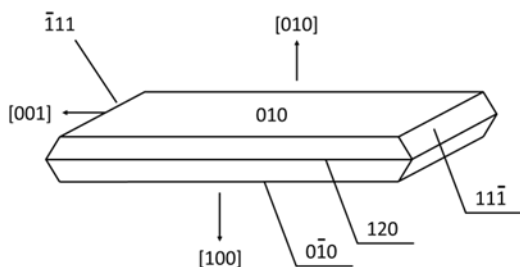
202   **Figure 2**   Crystal morphology of CaSO₄ [41].

203
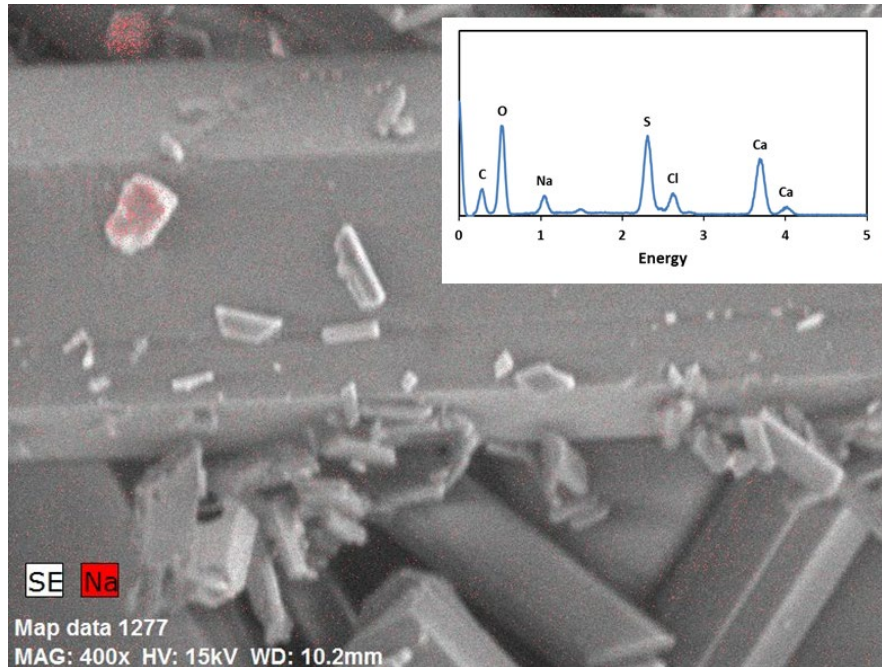
(a) SEM-EDX analysis
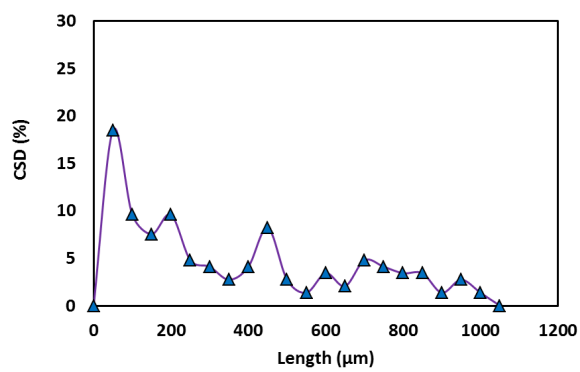
(b) CSD 'Length [001]'
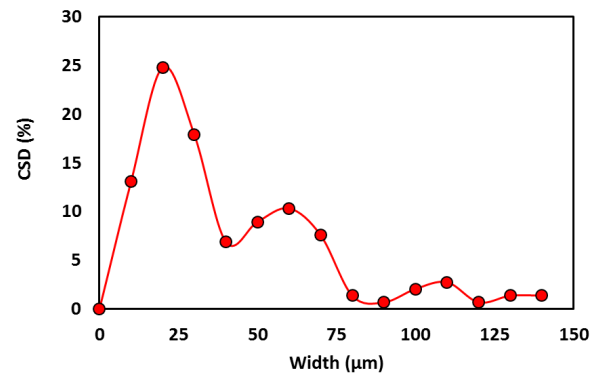
(c) CSD 'Width [100]'

204 **Figure 3** SEM-EDX analysis and CSD analysis of CaSO$_4$ crystal that was formed during

205 the batch crystallization experiment.

206

3.2. Influence of chemical factors

3.2.1. pH and Temperature

209 The influence of solution temperature (50 °C, 60 °C, and 80 °C) and pH (5 to 9) on

210 CaSO$_4$ crystallization was evaluated in terms of crystal CSD as well as the Ca^{2+} crystal

211 formation rate. The results showed that an increase in the heating temperature aided in

212 achieving higher Ca^{2+} reduction/removal efficiency (**Figure 4**). Conversely, there was no

213 distinct trend of Ca^{2+} removal efficiency at different pH ranges (**Figure 4**). For example, at

214 50°C, the Ca^{2+} removal at pH 9 was only 1.5% higher than that at pH 5. The results established

215 that the influence of an increase in the solution temperature on the formation of CaSO$_4$

216 exceeded that of the solution pH value. This was attributed to the change in solubility with

217 increases in the temperature.
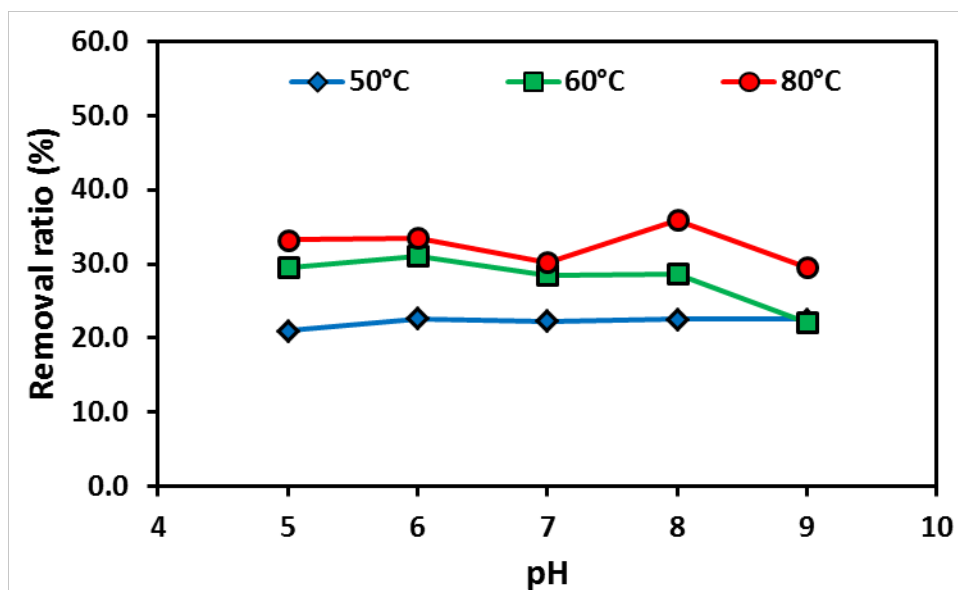
218

219   **Figure 4**   Reduction efficiency of calcium ions in the feed solution after crystallization.

220   A trend of broader CSD was observed at higher temperatures (**Figure 5 (a)** and **(b)**).

221   For example, at a heating temperature of 50 °C, CSD was in the range of 50 to 900 μm while

222   it ranged from 50 to 1,400 μm at 80 °C. With the increase in the heating temperature from

223   50 °C to 80 °C, the average crystal size increased, and the ratio of the small crystal that were

224   formed decreased. This tendency is similar to CaSO$_4$ solubility at different temperatures.

225   Specifically, CaSO$_4$ exhibits a lower solubility at temperatures exceeding 40 °C [42]. It was

226   expected that solubility is an important factor in the formation and growth of CaSO$_4$ crystals.

227   In the case of pH, with respect to high pH values of the feed solution, CSD exceeded the low

228   pH values (**Figure 5 (c) and (d)**). This was especially evident in the case of the CSD width.

229   For example, at the same heating temperature of 60 °C, the CSD width at pH 5 ranged from 50

230   μm to 650 μm while it ranged from 50 μm to 1150 μm at pH 9. Moreover, the portion of small

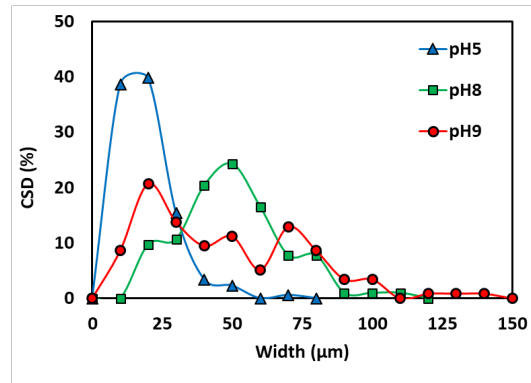231   size crystals at a high pH value was lower than that at a low pH value
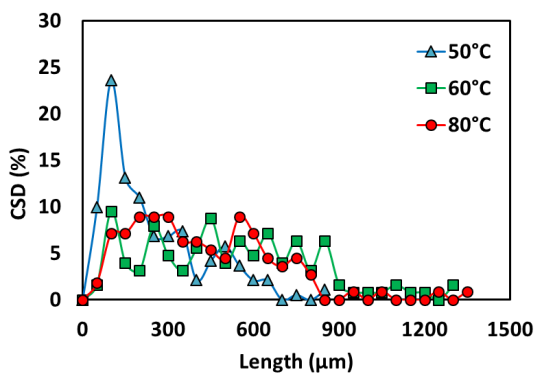
(a) Length [001] relative to temperature   (b) Width [100] relative to temperature
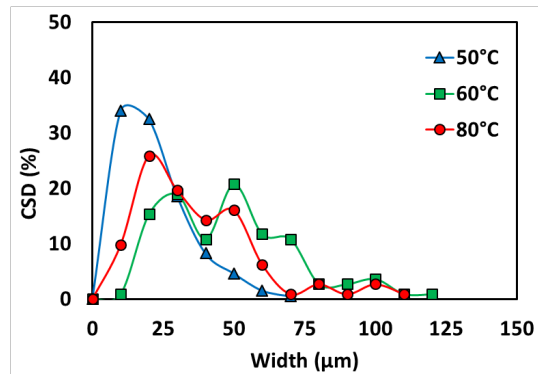
14
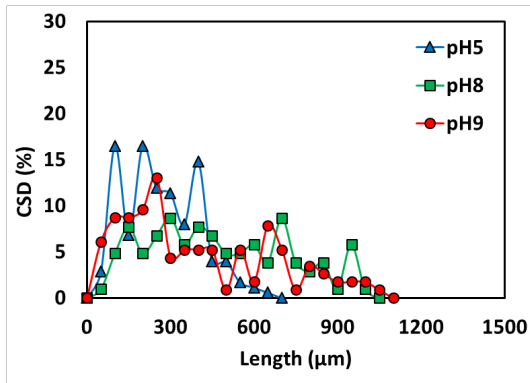
(c) Length [001] relative to pH   (d) Width [100] relative to pH

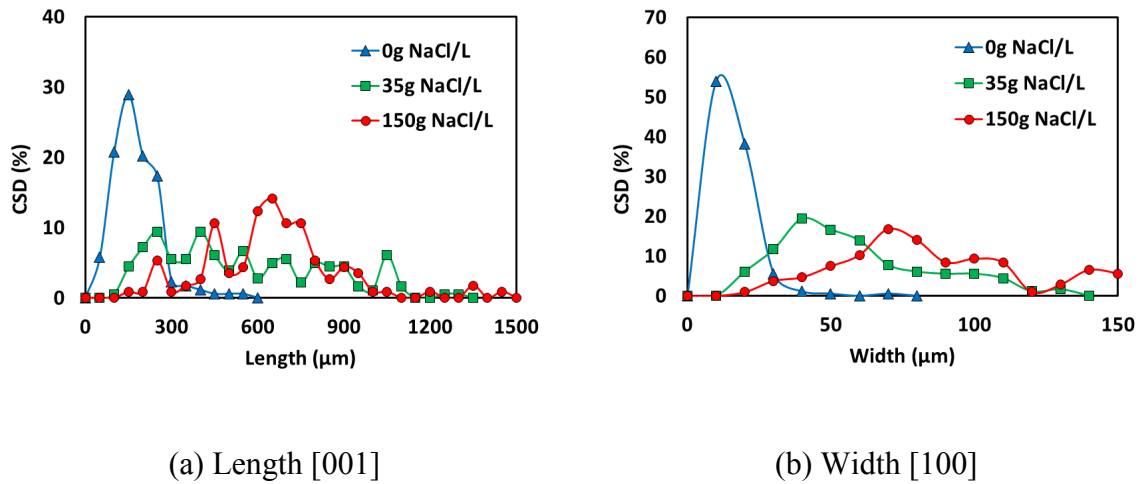**Figure 5**   Crystal size distribution (CSD) at different heating temperatures and pH values.

3.2.2 Concentration of NaCl

Actual seawater brine solution is highly saline with a NaCl concentration in the range of 35 g/L to 55 g/L. Thus, it is important to evaluate the influence of salinity on the formation of $CaSO_4$. The tendency of $CaSO_4$ formation in the presence of NaCl (35 g/L and 150 g/L) and in absence of NaCl were examined at a fixed pH of 7 and a temperature of 60 °C.

The presence of salt reduced the formation of the $CaSO_4$ crystal. The solution containing 35 g NaCl/L to 150 g NaCl/L resulted in 33.1% to 35.3% of Ca^{2+} removal efficiency. Comparatively, Ca^{2+} removal efficiency was 69.7% in the absence of NaCl. The influence of NaCl in reducing the formation of $CaSO_4$ was attributed to the ionic interference of Na^+ and Cl^-.

In terms of CSD, the presence of NaCl increased the size of $CaSO_4$ crystals that were formed. As shown in **Figure 6**, in the absence of NaCl in the solution, relatively small crystals were observed (both "Length" and "Width"). In comparison, in the presence of NaCl in the

15

247 solution, CSD in both directions were higher, and the dominant crystal size increased. Thus,

248 the CaSO$_4$ crystal size increased with increases in the NaCl concentration.

(a) Length [001]   (b) Width [100]

249 **Figure 6** Crystal Size Distribution (CSD) with different salt concentrations in the feed

250 solution.

251

252 **3.2.3 Effect of inorganic ions.**

253 **3.2.3.1 Sole ion**

254 The addition of inorganic ions, such as Mg^{2+}, K$^+$, and HCO$_3^-$, in the solution led to the

255 growth of other crystals with CaSO$_4$ crystals (**Figure 7**). The EDX analysis indicated that Na$^+$

256 was detected in the crystals that were formed along with Ca^{2+} and SO$_4^{2-}$ with the addition of

257 Mg^{2+} in the solution (**Figure 7 (a)**). Nevertheless, Mg^{2+} peaks were not detected in the EDX

258 spectral. However, the addition of Mg^{2+} resulted in a significantly reduced Ca^{2+} removal

259 efficiency (19.8±0.2%) when compared to the solution without any ion additions (29.5±0.6%)

260 (**Figure 8**). The results implied that Mg^{2+} affected the formation of CaSO$_4$ crystals.

261 Theoretically, Mg^{2+} can also combine with SO$_4^{2-}$ in the solution and precipitate in the form of

16

262 crystal (magnesium sulfate ($MgSO_4$)). The electronegativity influences a combination of

263 covalent linkages [43]. It is a measure of the tendency of an atom to attract a bonding a pair of

264 electrons. Specifically, the electronegativity of Mg^{2+} exceeds that of Ca^{2+} (Mg^{2+}: 1.31 vs Ca^{2+}:

265 1.00) [43, 44]. Hence, the ionic bonding force of Mg^{2+} with electrons exceeds that of Ca^{2+}.

266 Thus, an amount of SO_4^{2-} that can be combined with Ca^{2+} decreased because SO_4^{2-} was

267 attracted by Mg^{2+}. However, Mg^{2+} did not form crystals with SO_4^{2+} due to its much higher

268 solubility when compared with that of a $CaSO_4$ crystal. The solubility of $MgSO_4$ (351 g/L @

269 20 °C, 548 g/L @ 60 °C) significantly exceeds that of $CaSO_4$ (2.55 g/L @ 20 °C, 2.44 g/L @

270 60 °C) [45, 46]. This is used to account for the reduction in $CaSO_4$ crystals production.

271 Therefore, it is necessary to consider the same since a high quantity of Mg^{2+} presents in the

272 feed (0.22M as Mg^{2+}) simulated the SWRO brine.

273 The EDX analysis showed that the addition of K^+ to the solution did not change the

274 $CaSO_4$ crystal formation (**Figure 7 (b)**). Similarly, the addition of K^+ did not significantly

275 change the Ca^{2+} removal efficiency, and thus the Ca^{2+} removal efficiency remained in the range

276 of 32±1%, and it was closely similar to the solution without any added ions. The presence of

277 K^+ did not significantly influence the $CaSO_4$ formation due to its lower electronegativity (0.82).

278 Furthermore, when HCO_3^- ions were added to the bulk solution, the other crystals

279 formed in a globular form were observed in conjunction with $CaSO_4$ crystals. The EDX

280 mapping image showed that they did not contain Na^+ and Ca^{2+} in the globular crystals (**Figure**

281 **7 (c)**). Thus, the crystals with a globular shape were neither NaCl crystals nor $CaSO_4$ crystals.

282 Nevertheless, the addition of HCO_3^- to the solution did not significantly change the Ca^{2+}

283 removal efficiency, and therefore the Ca^{2+} removal efficiency remained in the range of

284 30.5±1.7% that was similar to that of the solution without any additional ions (**Figure 8**).
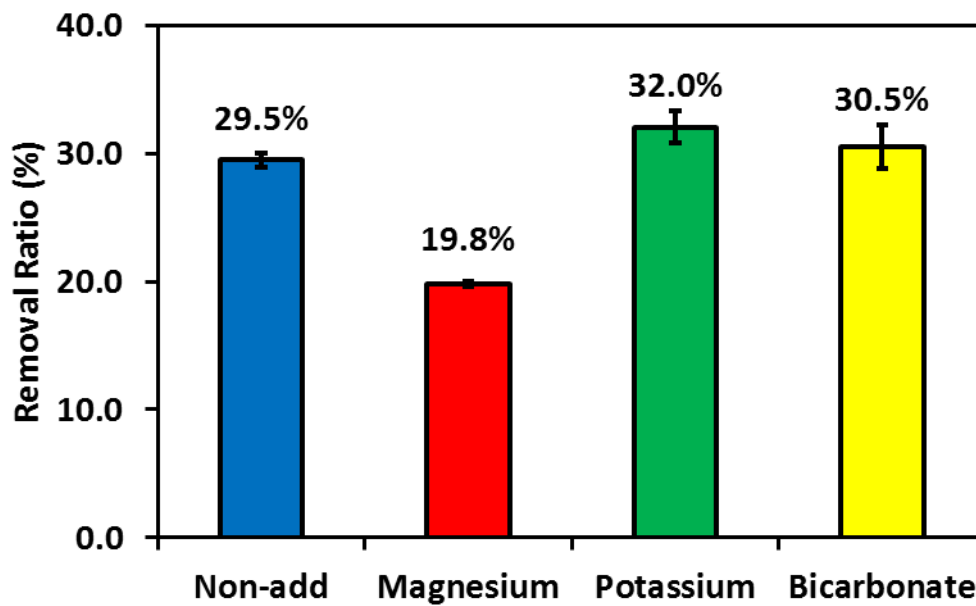
285
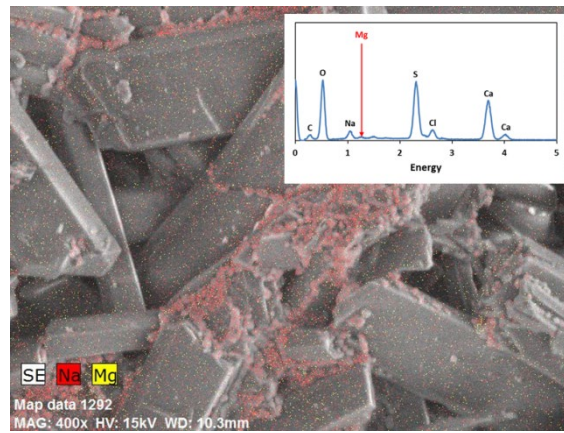
(a) Calcium with the addition of magnesium
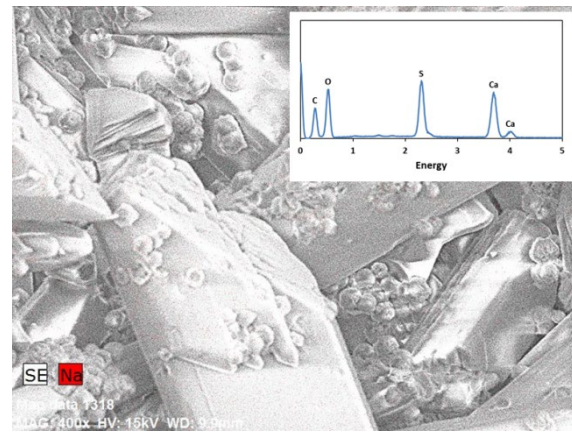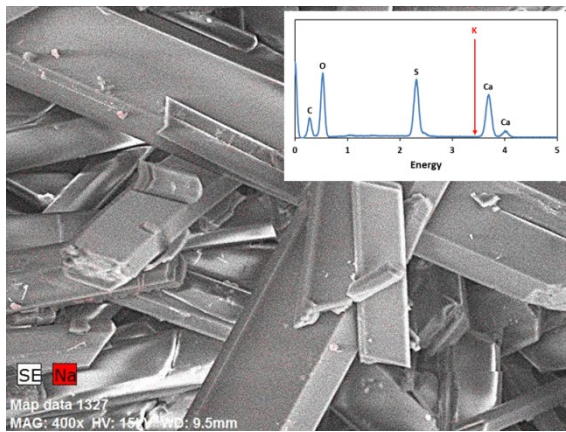
(b) Calcium with the addition of potassium

(c) Calcium with the addition of bicarbonate

286 **Figure 7**   SEM-EDX data of crystal shape and components with the addition of ions at 60

287 °C.

288

289 **Figure 8** The reduction efficiency of calcium ions in the feed solution after crystallization

290 with the addition of inorganic ions.

291

292 At the same heating temperature (60 °C), the CSD differed based on the existence of

293 specific ion in the feed solution. The CSD was higher when other ions were not added into the

294 feed solution; and the CSD ranged from 50 μm to 1,200 μm (**Figure 10**). However, when K^+,

295 Mg^{2+} and HCO_3^- were incorporated, the CSD ranged from 50 μm to 800 μm (with K^+), from

296 50 μm to 850 μm (with Mg^{2+}), and from 50 μm to 900 μm (with HCO_3^-). This implies that

297 these ions influenced the growth of $CaSO_4$ crystal. Thus, the ions interfere with the growth of

298 $CaSO_4$ crystals.

299
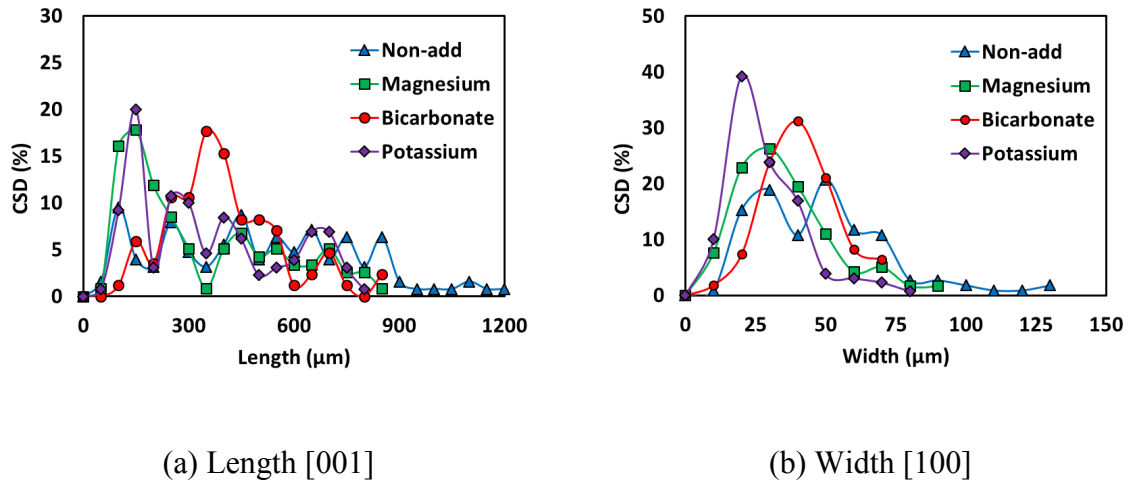
(a) Length [001]　　　　　　　　　　　　(b) Width [100]

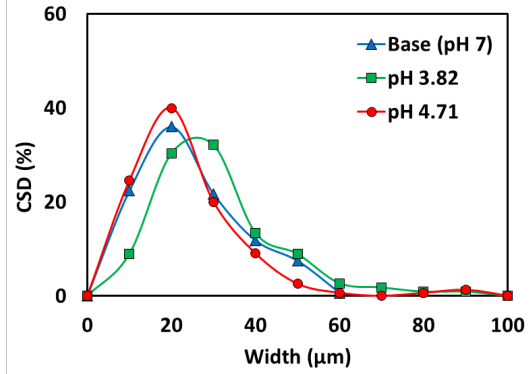**Figure 9**　　　　Crystal size distribution (CSD) with the addition of inorganic ions.

3.2.3.2 Chemical washing agents

In the SWRO process, chemical washing agents are employed to remove organic fouling, biofilm, and inorganic scaling [47]. The chemicals remain in the wastewater from SWRO process and are subsequently treated together with the SWRO brine. The presence of these chemicals in the SWRO brine may play a role in influencing the growth and size of $CaSO_4$ crystal formation. In the study, the changes in $CaSO_4$ crystal formation in the presence of EDTA chemical washing in the solution and at a fixed temperature of 60 °C and a stirring speed of 50 rpm was evaluated. The pH value of solution changed due to the addition of EDTA (pH 3.82 and 4.71). As shown in **Figure 10**, this did not significantly influence the formation and growth of crystals (27.01±0.53%) with addition of EDTA. The CSD and calcium ion rejection were almost similar in the absence and presence of EDTA (26.54%).

20
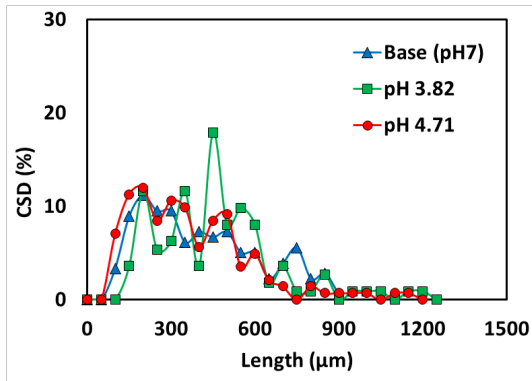
<center>(a) Length [001] with EDTA   (b) Width [100] with EDTA</center>

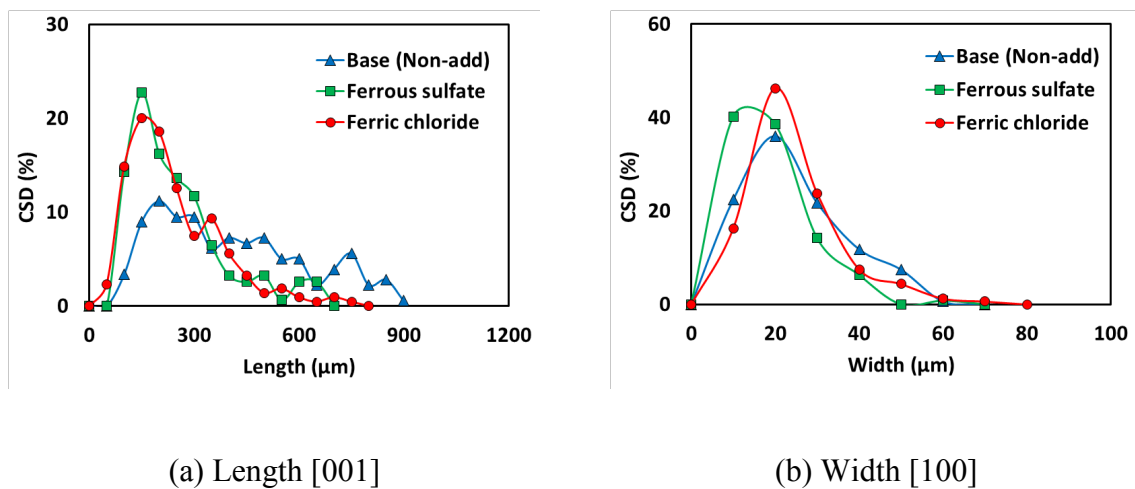313   **Figure 10**   Crystal size distribution (CSD) with chemical washing agent.

314

315   **3.2.3.3 Coagulation chemicals for pre-treatment**

316   Flocculation is often used as a pre-treatment for RO process to remove colloidal and

317   dissolved organic foulants. $FeSO_4$ and $FeCl_3$ are widely used as coagulants. In the study, the

318   effect of these two coagulants on $CaSO_4$ crystallization was investigated at a fixed pH of 7 and

319   a temperature of 60 °C. As shown in **Figure 11**, the CSD of $CaSO_4$ was affected by the presence

320   of both the coagulants ($FeSO_4$ and $FeCl_3$). In the case of the "Length" direction, the CSD

321   became narrow, and small crystals were detected in presence of coagulants. However, it did

322   not influence the CSD of the "Width" direction. Iron and chloride ions were not detected in the

323   crystals that were formed (**Figure 13**). As mentioned in section **3.1.3.1**, the added ions can be

324   combined with other ions in the formation of crystals. For example, the addition of Mg^{2+}

325   influences $CaSO_4$ crystal formation (**Figure 9**). However, Fe^{2+} did not influence it although

326   iron ions exhibit a higher electronegativity when compared with magnesium and calcium ions

327   (Fe^{3+}: 1.83, Mg^{2+}: 1.31, Ca^{2+}: 1.00). It is expected that concentration of iron ion is not

328   sufficiently high to influence the ionic bond force with sulfate ions (2.0 mM as Fe^{3+} in feed).

<center>21</center>

329   In case of the magnesium ions, a very high amount of magnesium ions was added into the feed

330   (0.22 M as Mg^{2+}). Additionally, the solubility of $FeSO_4$ and $FeCl_3$ significantly exceeds that of

331    $CaSO_4$ ($FeSO_4$: 256 g/L @ 20 °C, and $FeCl_3$: 920 g/L @ 20 °C).

332   In terms of the formations of crystal, each coagulant exhibits a different effect. When

333    $FeCl_3$ was added, the amount of calcium that was rejected was almost same (27.9%) as that

334   given the non-addition of coagulant (28.5%). Conversely, the rejection ratio of calcium ions

335   (42.7%) increased when $FeSO_4$ was added. This indicates that $FeSO_4$ simulates the formation

336   of crystals due to the presence of sulfate ions. The results indicated that the addition of sulfate

337   ions influenced the formation of $CaSO_4$ crystal. Increased $CaSO_4$ crystals were formed in the

338   presence of SO_4^{2-} in the feed solution. Overall, both the coagulant chemicals negatively

339   influenced crystal growth in the "Length" direction.

(a) Length [001]   (b) Width [100]

340   **Figure 11**   Crystal Size distribution (CSD) of $CaSO_4$ in the presence of a coagulant.

341
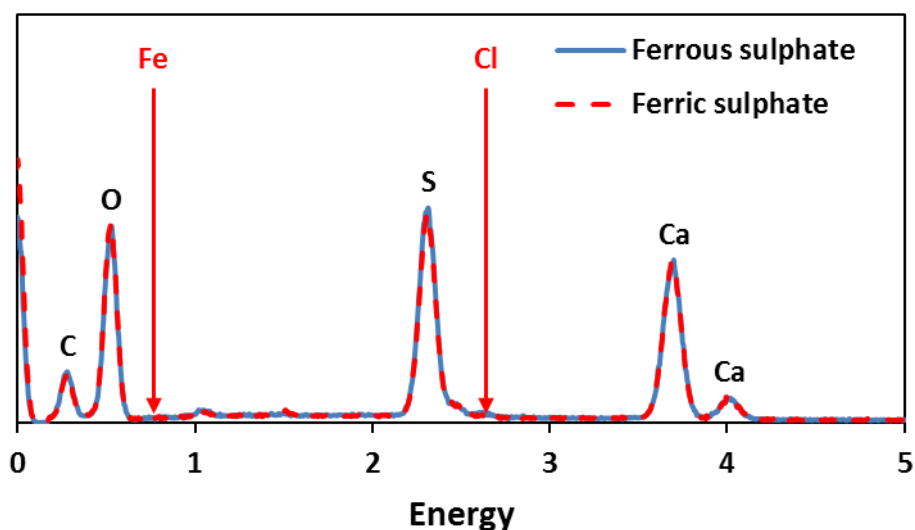
Figure 12   EDX data of CaSO$_4$ crystals in the presence of a coagulant.

343

3.3. Effect of organic matter

345   Organic matters, such as polysaccharide, protein, and humic, are found in seawater and

346   SWRO brine. Here, HA, BSA, and AA represent the humic, proteins, and polysaccharide (the

347   common model organic foulant in brine). As shown in **Figure 13**, when organic matters (HA,

348   BSA and AA) are added in a feed solution, the CSD in the "Length" direction became narrower,

349   and the dominant crystals size became smaller. In contrast, CSD (in "Width" direction) did not

350   change significantly with the addition of organic matters. This revealed that all three organic

351   matters that were used prevented the growth of crystals in the length direction. In the case of

352   the HA addition, the rejection ratio of Ca^{2+} increased to approximately 10% although they did

353   not influence the growth of crystals (Ca^{2+} rejection efficiency: 29.0% @ Non-addition, 38.5%

354   @ addition of HA, 30.8% @ addition of AA, 31.1% @ addition of BSA). This is potentially

355   due to the reduction of electrostatic repulsion between Ca^{2+} [48, 49]. Additionally, HA

23

356 possesses a negative charge [50]. It plays the role of a bridge between Ca^{2+} and HA (bridging

357 effect and/or complexation). Hence, Ca^{2+} adsorbs onto the HA compound. It causes a higher

358 rejection of the Ca^{2+} in a solution than the Ca^{2+} rejection ratio given non-addition.

(a) Length [001]   (b) Width [100]
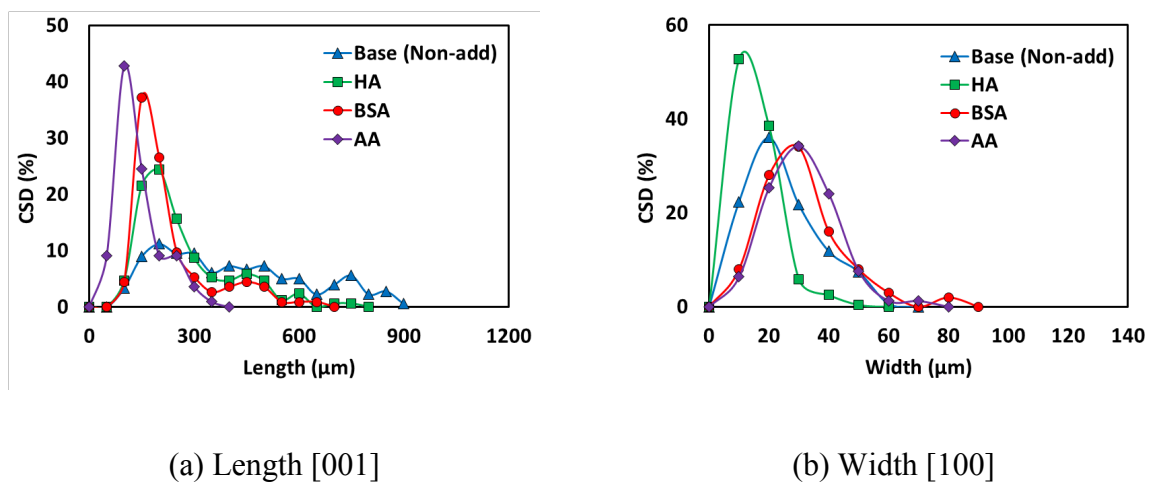
359 **Figure 13**   Crystal Size Distribution (CSD) in the presence of organic matter.

360 **Table 2** Calcium ion rejection efficiency in presence of organic matter.

| Organic matter	Calcium rejection efficiency (%)
No addition	29.01
Humic acid (HA)	38.45
Alginate (AA)	30.76
Bovine serum albumin (BSA)	31.13

361

3.4. Effect of physical factors

363   In the submerged membrane process, physical methods, such as agitation, aeration, and

364 vibration are applied to reduce the fouling phenomenon and to agitate (mix) the solution [51].

365 Additionally, the crystallization tendency is significantly influenced by physical factors such

366 as agitation speed. Furthermore, it is important to operate the crystallizer at an appropriate

24

367   agitation speed [35, 52]. In this section, three different agitation speeds (0 rpm, 20 rpm (as the

368   lower speed), and 150 rpm (as the higher speed)) were applied.

369   As shown in **Figure 14**, CSD was influenced by the agitation intensity (or mixing

370   speed). The dominant crystals size of CSD increases in the "Length" direction when the

371   agitation intensity increased. This indicates that the hydrodynamic conditions are more suitable

372   for crystal growth at a higher agitation intensity. In this case, a better suspension of crystals

373   was provided by higher agitation intensity. Thus, the surface area that is exposed to the solution

374   for mass transfer between crystal surface and solution increased. As shown in **Figure 15**,

375   suspension crystals in the solution were evenly distributed with higher agitation intensity. In

376   comparison, crystals were formed towards the bottom side at a lower agitation intensity.

377   However, in the case of the "Width" direction, the dominant size of crystal increases at the low

378   mixing speed of 20 rpm although the dominant size decreased at a higher agitation intensity.

379   This may be due to crystal breakage that is caused by collisions between crystals and impeller

380   of jar-tester or wall of batch cell [35]. At a higher agitation speed, the probability of collision

381   of crystals increased with increases in the collision power. This can lead to a higher degree of

382   breakage of crystals. A lower dominant size of crystals at higher agitation intensity was

383   detected in the case of the "Width" direction. It is assumed that the crystal side of the "Width"

384   direction (side 120) exhibits a weaker solidity when compared with the dimension of "Length"

385   direction (side $\bar{1}11$) **(Figure 2)**. At a high mixing, the increase in the effective surface of the

386   crystal, which is contacted to solution, increases the formation ratio of crystals. However, the

387   formation ratio is not significantly different at lower (20 rpm) and higher (150 rpm) agitation

388   intensities (Ca^{2+} rejection ratio: 11.7% @ 0 rpm, 27.2% @ 20 rpm, and 28.9% @ 150 rpm).
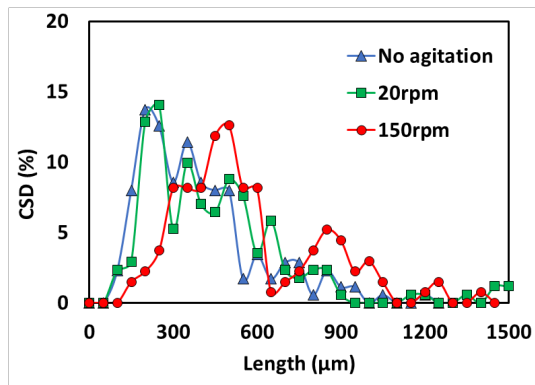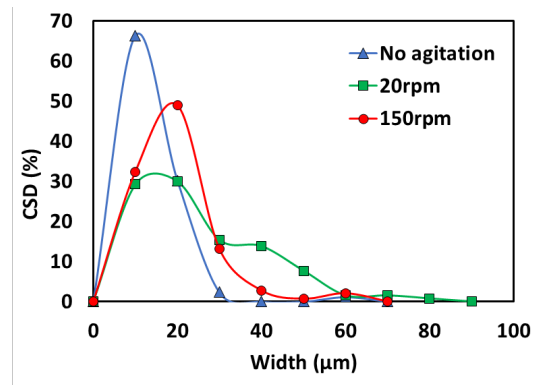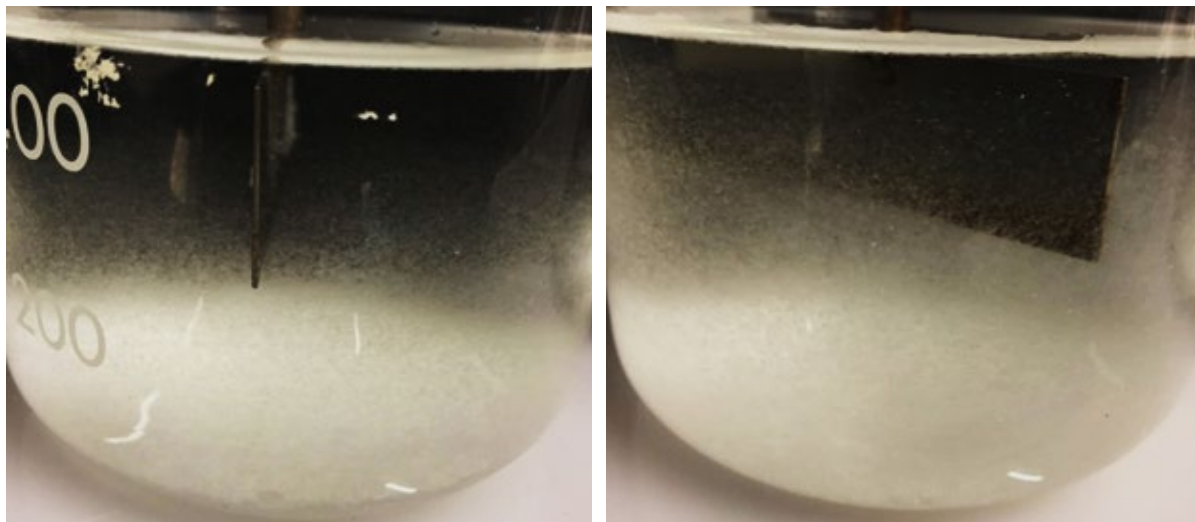
(a) Length [001]　　　　　　　　　　　(b) Width [100]

389　**Figure 14**　　Crystal Size Distribution (CSD) at different mixing velocities.

(a) At lower agitation intensity (20 rpm)　　(b) At higher agitation intensity (150 rpm)

390　**Figure 15**　　Suspension of crystals at different agitation intensities.

4. Conclusions

In this study, the crystallization tendency of $CaSO_4$ in saline solution was examined with different factors at the same standard condition such as chemical factors (temperature, pH, NaCl concentration, and chemical agents), organic matters (AA, HA and BSA) and physical factors (agitation). It is important to possess a good understanding of the suitable control of chemical and physical factors for crystal formation in the MDC process. Crystallization is an effective approach to reduce scaling and fouling and to recover valuable resources from brine. Based on the results of this study, the following conclusions were obtained:

- The size and amount of $CaSO_4$ crystals increased at a higher solution temperature. At the increased solution temperature (80 °C), 32.5±2.6% Ca removal efficiency was achieved when compared to 22.2±0.7% at a lower temperature (50 °C). The pH did not play a significant role in the amount of $CaSO_4$ that was formed but a higher pH enabled an increase in the size of $CaSO_4$ crystals

- The presence of NaCl reduced the formation of $CaSO_4$ and the Ca^{2+} removal efficiency was reduced.

- The presence of Mg^{2+} reduced the Ca^{2+} removal efficiency, and this is attributed to the strong electronegativity of Mg^{2+} when compared to that of Ca^{2+}. The presence of K^+ and HCO_3^- did not play a significant role in the $CaSO_4$ formation. In comparison, $FeSO_4$ stimulates the formation of $CaSO_4$ crystal because it includes a SO_4^{2+}.

- In the presence of organic matter, the CSD in the "Length" direction decreased, and the formation of crystal was slightly improved. In the presence of HA, the Ca^{2+} rejection increased by bridging the effect between Ca^{2+} and HA.

413   • Agitation positively affects the formation and growth of crystals, and it is controlled by

414   adjusting the agitation intensity. A higher agitation intensity (150 rpm) is suitable

415   because it provides a sufficient suspension of crystals.

416

417 **Acknowledgement**

420

421

References

[1] A. Pérez-González, A.M. Urtiaga, R. Ibáñez, I. Ortiz, State of the art and review on the treatment technologies of water reverse osmosis concentrates, Water Research, 46 (2012) 267-283.

[2] C.R. Acevedo, J.L. Gardea-Torresdey, A.J. Tarquin, Silica Removal from Brine by Using Ion Exchange, in: World Environmental and Water Resources Congress 2010, 2010.

[3] F. Edwie, T.-S. Chung, Development of hollow fiber membranes for water and salt recovery from highly concentrated brine via direct contact membrane distillation and crystallization, Journal of Membrane Science, 421–422 (2012) 111-123.

[4] D.A. Roberts, E.L. Johnston, N.A. Knott, Impacts of desalination plant discharges on the marine environment: A critical review of published studies, Water Research, 44 (2010) 5117-5128.

[5] A.M.O. Mohamed, M. Maraqa, J. Al Handhaly, Impact of land disposal of reject brine from desalination plants on soil and groundwater, Desalination, 182 (2005) 411-433.

[6] S. Loeb, Production of energy from concentrated brines by pressure-retarded osmosis : I. Preliminary technical and economic correlations, Journal of Membrane Science, 1 (1976) 49-63.

[7] S. Loeb, F. Van Hessen, D. Shahaf, Production of energy from concentrated brines by pressure-retarded osmosis : II. Experimental results and projected energy costs, Journal of Membrane Science, 1 (1976) 249-269.

[8] H. Sakai, T. Ueyama, M. Irie, K. Matsuyama, A. Tanioka, K. Saito, A. Kumano, Energy recovery by PRO in sea water desalination plant, Desalination, 389 (2016) 52-57.

[9] Y. Choi, S. Vigneswaran, S. Lee, Evaluation of fouling potential and power density in pressure retarded osmosis (PRO) by fouling index, Desalination, 389 (2016) 215-223.

[10] D.L. Shaffer, N.Y. Yip, J. Gilron, M. Elimelech, Seawater desalination for agriculture by integrated forward and reverse osmosis: Improved product water quality for potentially less energy, Journal of Membrane Science, 415–416 (2012) 1-8.

[11] C.R. Martinetti, A.E. Childress, T.Y. Cath, High recovery of concentrated RO brines using forward osmosis and membrane distillation, Journal of Membrane Science, 331 (2009) 31-39.

[12] R. Bouchrit, A. Boubakri, A. Hafiane, S.A.-T. Bouguecha, Direct contact membrane distillation: Capability to treat hyper-saline solution, Desalination, 376 (2015) 117-129.

[13] E. Curcio, X. Ji, G. Di Profio, A.O. Sulaiman, E. Fontananova, E. Drioli, Membrane distillation operated at high seawater concentration factors: Role of the membrane on CaCO3 scaling in presence of humic acid, Journal of Membrane Science, 346 (2010) 263-269.

456   [14] M. Gryta, The study of performance of polyethylene chlorinetrifluoroethylene membranes
457   used for brine desalination by membrane distillation, Desalination, 398 (2016) 52-63.

458   [15] E. Curcio, E. Drioli, Membrane Distillation and Related Operations—A Review,
459   Separation & Purification Reviews, 34 (2005) 35-86.

460   [16] G. Naidu, S. Jeong, Y. Choi, S. Vigneswaran, Membrane distillation for wastewater
461   reverse osmosis concentrate treatment with water reuse potential, Journal of Membrane
462   Science, 524 (2017) 565-575.

463   [17] G. Naidu, W.G. Shim, S. Jeong, Y. Choi, N. Ghaffour, S. Vigneswaran, Transport
464   phenomena and fouling in vacuum enhanced direct contact membrane distillation:
465   Experimental and modelling, Separation and Purification Technology, 172 (2017) 285-295.

466   [18] K.W. Lawson, D.R. Lloyd, Membrane distillation, Journal of Membrane Science, 124
467   (1997) 1-25.

468   [19] Y. Shin, J. Sohn, Mechanisms for scale formation in simultaneous membrane distillation
469   crystallization: Effect of flow rate, Journal of Industrial and Engineering Chemistry, 35 (2016)
470   318-324.

471   [20] F. Edwie, T.-S. Chung, Development of simultaneous membrane distillation–
472   crystallization (SMDC) technology for treatment of saturated brine, Chemical Engineering
473   Science, 98 (2013) 160-172.

474   [21] C.M. Tun, A.G. Fane, J.T. Matheickal, R. Sheikholeslami, Membrane distillation
475   crystallization of concentrated salts—flux and crystal formation, Journal of Membrane Science,
476   257 (2005) 144-155.

477   [22] C.A. Quist-Jensen, A. Ali, S. Mondal, F. Macedonio, E. Drioli, A study of membrane
478   distillation and crystallization for lithium recovery from high-concentrated aqueous solutions,
479   Journal of Membrane Science, 505 (2016) 167-173.

480   [23] C.A. Quist-Jensen, F. Macedonio, E. Drioli, Membrane crystallization for salts recovery
481   from brine—an experimental and theoretical analysis, Desalination and Water Treatment, 57
482   (2016) 7593-7603.

483   [24] A. Giwa, V. Dufour, F. Al Marzooqi, M. Al Kaabi, S.W. Hasan, Brine management
484   methods: Recent innovations and current status, Desalination, 407 (2017) 1-23.

485   [25] F. Anisi, K.M. Thomas, H.J.M. Kramer, Membrane-assisted crystallization: Membrane
486   characterization, modelling and experiments, Chemical Engineering Science, 158 (2017) 277-
487   286.

488   [26] G. Guan, R. Wang, F. Wicaksana, X. Yang, A.G. Fane, Analysis of Membrane Distillation
489   Crystallization System for High Salinity Brine Treatment with Zero Discharge Using Aspen
490   Flowsheet Simulation, Industrial & Engineering Chemistry Research, 51 (2012) 13405-13413.

491   [27] S. Goh, J. Zhang, Y. Liu, A.G. Fane, Fouling and wetting in membrane distillation (MD)
492   and MD-bioreactor (MDBR) for wastewater reclamation, Desalination, 323 (2013) 39-47.

493   [28] G. Naidu, S. Jeong, S. Vigneswaran, Influence of feed/permeate velocity on scaling
494   development in a direct contact membrane distillation, Separation and Purification Technology,
495   125 (2014) 291-300.

496   [29] J. Morillo, J. Usero, D. Rosado, H. El Bakouri, A. Riaza, F.-J. Bernaola, Comparative
497   study of brine management technologies for desalination plants, Desalination, 336 (2014) 32-
498   49.

499   [30] F. He, K.K. Sirkar, J. Gilron, Studies on scaling of membranes in desalination by direct
500   contact membrane distillation: CaCO3 and mixed CaCO3/CaSO4 systems, Chemical
501   Engineering Science, 64 (2009) 1844-1859.

502   [31] L.F. Greenlee, F. Testa, D.F. Lawler, B.D. Freeman, P. Moulin, Effect of antiscalant
503   degradation on salt precipitation and solid/liquid separation of RO concentrate, Journal of
504   Membrane Science, 366 (2011) 48-61.

505   [32] D. Squire, J. Murrer, P. Holden, C. Fitzpatrick, Disposal of reverse osmosis membrane
506   concentrate, Desalination, 108 (1997) 143-147.

507   [33] P. Chelme-Ayala, D.W. Smith, M.G. El-Din, Membrane concentrate management options:
508   a comprehensive critical reviewA paper submitted to the Journal of Environmental Engineering
509   and Science, Canadian Journal of Civil Engineering, 36 (2009) 1107-1119.

510   [34] A. Haghtalab, M.H. Badizad, Solubility of gypsum in aqueous NaCl + K2SO4 solution
511   using calcium ion selective electrode-investigation of ionic interactions, Fluid Phase Equilibria,
512   409 (2016) 341-353.

513   [35] M. Akrap, N. Kuzmanić, J. Prlić-Kardum, Effect of mixing on the crystal size distribution
514   of borax decahydrate in a batch cooling crystallizer, Journal of Crystal Growth, 312 (2010)
515   3603-3608.

516   [36] T. Waly, M.D. Kennedy, G.-J. Witkamp, G. Amy, J.C. Schippers, The role of inorganic
517   ions in the calcium carbonate scaling of seawater reverse osmosis systems, Desalination, 284
518   (2012) 279-287.

519   [37] T. Yu, L. Meng, Q.-B. Zhao, Y. Shi, H.-Y. Hu, Y. Lu, Effects of chemical cleaning on RO
520   membrane inorganic, organic and microbial foulant removal in a full-scale plant for municipal
521   wastewater reclamation, Water Research, 113 (2017) 1-10.

522   [38] W.S. Ang, N.Y. Yip, A. Tiraferri, M. Elimelech, Chemical cleaning of RO membranes
523   fouled by wastewater effluent: Achieving higher efficiency with dual-step cleaning, Journal of
524   Membrane Science, 382 (2011) 100-106.

525   [39] T. Nguyen, F.A. Roddick, L. Fan, Biofouling of Water Treatment Membranes: A Review
526   of the Underlying Causes, Monitoring Techniques and Control Measures, Membrane, 2 (2012)
527   804-840.

528 [40] C.J. Gabelich, T.I. Yun, B.M. Coffey, I.H.M. Suffet, Effects of aluminum sulfate and
529 ferric chloride coagulant residuals on polyamide membrane performance, Desalination, 150
530 (2002) 15-30.

531 [41] O.D. Linnikov, Investigation of the initial period of sulphate scale formation Part 2.
532 Kinetics of calcium sulphate crystal growth at its crystallization on a heat-exchange surface,
533 Desalination, 128 (2000) 35-46.

534 [42] G. Azimi, V.G. Papangelakis, The solubility of gypsum and anhydrite in simulated laterite
535 pressure acid leach solutions up to 250 °C, Hydrometallurgy, 102 (2010) 1-13.

536 [43] C.A. Boeyens Jan, The Periodic Electronegativity Table, in: Zeitschrift für
537 Naturforschung B, 2008, pp. 199.

538 [44] A.L. Allred, Electronegativity values from thermochemical data, Journal of Inorganic and
539 Nuclear Chemistry, 17 (1961) 215-221.

540 [45] W.L. Marshall, Aqueous systems at high temperature. XX. Dissociation constant and
541 thermodynamic functions for magnesium sulfate to 200.degree, The Journal of Physical
542 Chemistry, 71 (1967) 3584-3588.

543 [46] E.P. Partridge, A.H. White, THE SOLUBILITY OF CALCIUM SULFATE FROM 0 TO
544 200°, Journal of the American Chemical Society, 51 (1929) 360-370.

545 [47] S. Jeong, G. Naidu, R. Vollprecht, T. Leiknes, S. Vigneswaran, In-depth analyses of
546 organic matters in a full-scale seawater desalination plant and an autopsy of reverse osmosis
547 membrane, Separation and Purification Technology, 162 (2016) 171-179.

548 [48] G. Naidu, S. Jeong, S. Vigneswaran, Interaction of humic substances on fouling in
549 membrane distillation for seawater desalination, Chemical Engineering Journal, 262 (2015)
550 946-957.

551 [49] D. Jermann, W. Pronk, S. Meylan, M. Boller, Interplay of different NOM fouling
552 mechanisms during ultrafiltration for drinking water production, Water Research, 41 (2007)
553 1713-1722.

554 [50] K.L. Jones, C.R. O'Melia, Protein and humic acid adsorption onto hydrophilic membrane
555 surfaces: effects of pH and ionic strength, Journal of Membrane Science, 165 (2000) 31-46.

556 [51] N.V. Ndinisa, A.G. Fane, D.E. Wiley, Fouling Control in a Submerged Flat Sheet
557 Membrane System: Part I – Bubbling and Hydrodynamic Effects, Separation Science and
558 Technology, 41 (2006) 1383-1409.

559 [52] K. Shimizu, K. Takahashi, E. Suzuki, T. Nomura, Effect of baffle geometries on crystal
560 size distribution of aluminum potassium sulfate in a seeded batch crystallizer, Journal of
561 Crystal Growth, 197 (1999) 921-926.

562